SURF 2013

Characterization of Second Harmonics Generators for Advanced LIGO

Andres Medina, Bard College, Annandale-on-Hudson
Mentors: Sheila Dwyer and Dr. Daniel Sigg

Characterization of Second Harmonics Generators for Advanced LIGO Squeezing

Abstract:

The sensitivity of Initial LIGO gravitational interferometers wave detectors was fundamentally limited above a few hundred Hertz by quantum noise, namely shot noise. This noise can be reduced by increasing the laser power, or by implementing squeezed light. Squeezed light is a quantum phenomenon that results in the creation of two correlated photons. Having correlated photons reduces the standard deviation in their photon-counting statistic, which results in a decrease in the shot noise. One essential component in creating squeezed light is a second harmonic generator, which produces green light at twice the frequency of the interferometer laser. The aim of this paper is to characterize the second harmonic generator that might be used in Advanced LIGO. We measure the intra-cavity losses, characterize the locking of the cavity, and characterize the efficiency of conversion from infrared to green light.

Introduction:

The existence of gravitational waves (GWs) was first predicted by Albert Einstein in his general theory of relativity. In his theory, he predicted that accelerated mass quadrupoles, such as supernova explosions and black holes, can produce ripples in the spacetime curvature that propagate at the speed of light away from the object that generates them [9]. Based on general relativity, GWs are predicted to be transverse and quadrupolar in nature [9]. The same way as electromagnetic radiation, GWs have two polarizations, which interact weakly with matter. For instance, if we have a ring of free test masses, located on the x-y plane, and gravitational waves propagating on the z-axis, we would observe that the ring would get disturbed into an ellipse as shown in Figure 1.

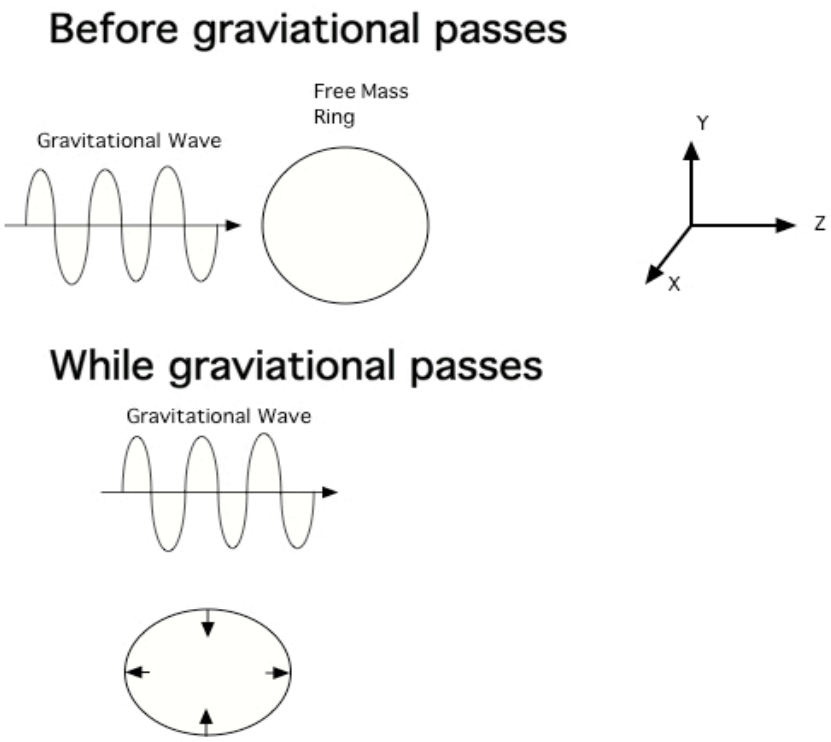

Figure 1. Gravitational wave traveling on the z direction and a ring of free masses on the x-y plane. The distortion of the ring that is created by the gravitational waves depends on the GWs polarization.

The strain that the gravitational waves would create on the ring of test masses depends on the GWs amplitude, which is given by the formula $\Delta L = hL$, where h is the amplitude of the GWs and L in our example is the diameter of the circle.

In order to detect GWs, two Laser Interferometer Gravitational-Wave Observatories (LIGO) were built: one in Hanford, WA, and the other one in Livingston, LA. These two observatories use a Michelson Interferometer of 4km long with quasi-free-falling mirrors. By using a Michelson Interferometer, in theory we would be able to detect GWs since GWs would interact with the quasi-free-falling mirror by stretching one arm and contracting the other arm [7]. However, GWs from sources such as supernovae or collision of neutron stars are predicted to have amplitudes of the order of 10^{-21}[7].

Gravitational wave detectors need to make extremely low noise measurements to detect these small signals with a good signal to noise ratio.

Since our gravitational wave detector is a Michelson Interferometer with a quasi-free-falling mirror, the quantum nature of electromagnetic waves imposes a fundamental limit on the sensitivity of the detector. This limitation is due to quantum noise namely photon counting noise or shot noise. Shot noise is due to the fact that photons are used in order to measure the change in the mirrors. There is an uncertainty associated with the number of photons that the detector detects. The uncertainty in the number of photons obeys Poisson statistics with an uncertainty given by $\sqrt{n}$, where n is the number of photons. One solution to shot noise is to increase the laser power. However, increasing the laser power produces another measurable noise namely radiation pressure noise [9]. Radiation pressure noise is the result of photons hitting the mirrors and randomly displacing them. Radiation pressure noise can be easily solved by increasing the weight of the quasi-free-falling mirrors. On the other hand, a better way to improve the sensitivity of the detector without increasing the laser power is to use something called squeezed light. Squeezed light is a quantum phenomenon that results in the creation of two correlated photons or entangled photons. Since second harmonic generator (SHG) is an essential component in the creation of squeezed light, we need to build and characterize a SHG suitable for an advanced LIGO squeezer.

I. Second Harmonic Generation:

Our second harmonic generator (SHG) is a device that consists on a nonlinear crystal, located at the center of the device, two mirrors, located at in each ends of the device, a PZT and a temperature controller. The Figure 2 below illustrates the second harmonic generator that we are using.

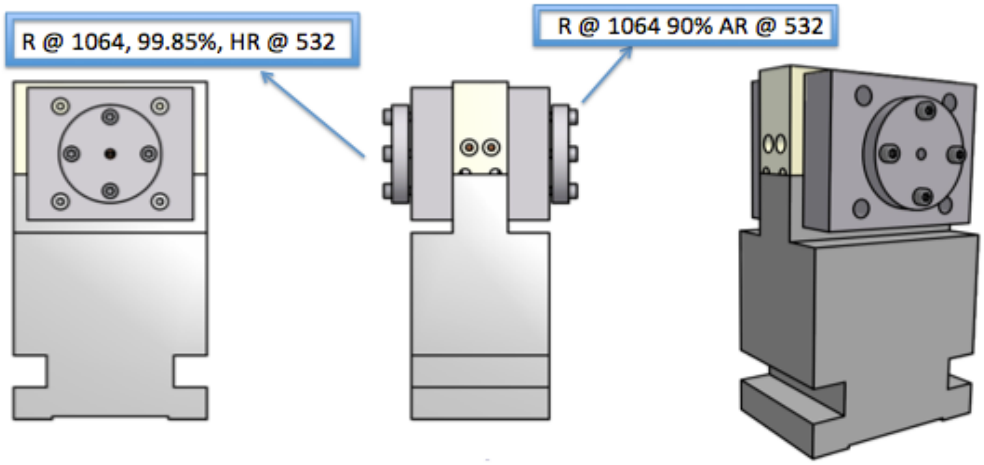

Figure 2. Second Harmonic Generator, designed at AEI Hannover, Germany.

Before we take a look at what happens inside the SHG, let's take a look at electromagnetic waves in matter. When electromagnetic waves propagate inside a dielectric medium, the electric field vector interacts with the charges in the dielectric material causing a displacement of charges as shown Figure 3. The displacement of charges results in an induced electric field that opposes the incoming electric field. This induced electric field inside the dielectric material is characterized by the **Polarization vector, P**, which is defined by the following formula $\boldsymbol{P} = \varepsilon_0 \chi^{(1)} \boldsymbol{E}$, where ε_0 is the free-space permittivity, and $\chi^{(1)}$ is the linear susceptibility [5].

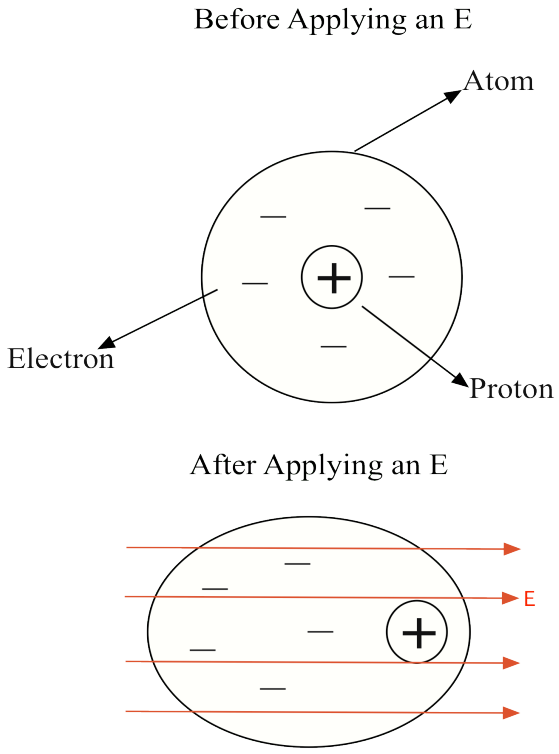

Figure 3a) A neutral atom before and after an applied electric field.

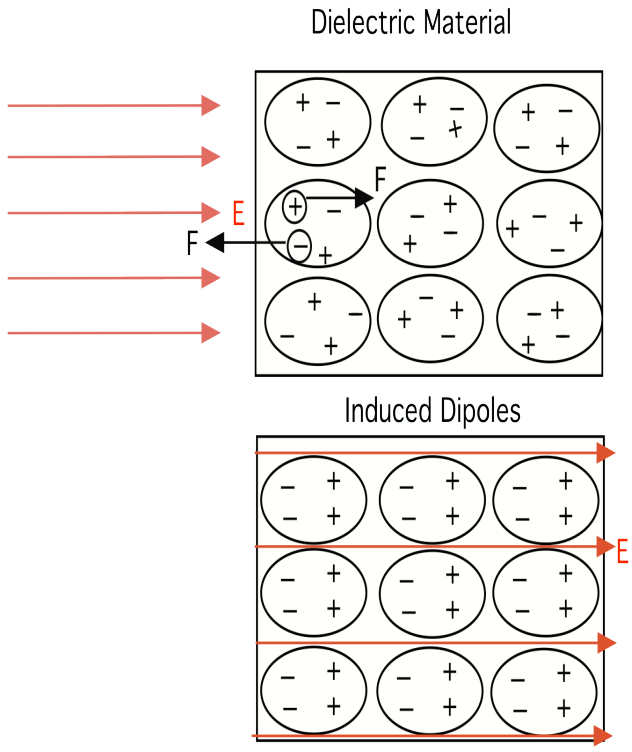

Figure 3b) A dielectric material in the present of an electric field.

In linear optics, **P** depends linearly on the electric field, which means that an increasing in the electric field results in an increasing **P**. In nonlinear optics, the **P** does not obey linearity but instead the polarization vector is a power series expansion of the electric field, which is given by

$$\boldsymbol{P}(t) = \varepsilon_0\left[\chi^{(1)}\boldsymbol{E}(t) + \chi^{(2)}\boldsymbol{E^2}(t) + \chi^{(3)}\boldsymbol{E^3}(t) + \cdots\right] \equiv \boldsymbol{P^{(1)}}(t) + \boldsymbol{P^{(2)}}(t) + \boldsymbol{P^{(3)}}(t) + \cdots$$

where $\chi^{(2)}$ and $\chi^{(3)}$ are known as the second and third nonlinear optical susceptibilities[2]. The term $\boldsymbol{P^{(2)}}(t) = \chi^{(2)}\boldsymbol{E^2}(t)$ is referred as the second order nonlinear polarization vector, and this term is the one responsible for second harmonic generation in non-centrosymmetrical crystals or crystals that do not have inversion

symmetry [2]. Now, let's imagine that we have an incident electric field in a non-centrosymmetrical crystal whose electric field is given by:

$$\boldsymbol{E}(t) = \boldsymbol{E}e^{-i\omega t} + \boldsymbol{E}^{*}e^{i\omega t}$$

Let's take the expression for the second order nonlinear polarization vector and substitute the electric field:

$$\boldsymbol{P^{(2)}}(t) = \varepsilon_0\chi^{(2)}\boldsymbol{E}(\boldsymbol{t})^{\boldsymbol{2}}$$

$$\boldsymbol{P^{2}}(t) = \varepsilon_0\chi^{(2)}\left[\boldsymbol{E}e^{-i\omega t} + \boldsymbol{E}^{*}e^{i\omega t}\right]^{\boldsymbol{2}}$$

$$= \varepsilon_0\chi^{(2)}\left[\boldsymbol{E^{2}}e^{-2i\omega t} + 2\boldsymbol{E}\boldsymbol{E}^{*} + \left(\boldsymbol{E}^{*}\right)^{\boldsymbol{2}}e^{2i\omega t}\right]$$

$$= 2\varepsilon_0\chi^{(2)}\boldsymbol{E}\boldsymbol{E}^{*} + \varepsilon_0\chi^{(2)}\left[\boldsymbol{E^{2}}e^{-2i\omega t} + \left(\boldsymbol{E}^{*}\right)^{\boldsymbol{2}}e^{2i\omega t}\right]$$

In the formula above, we can observe the generation of a frequency 2ω, which is second harmonic generation. In other words, second harmonic generation is the process in which monochromatic coherent wave of frequency ω induced a coherent wave emission of frequency 2ω as illustrated in the Figure 4 [5].

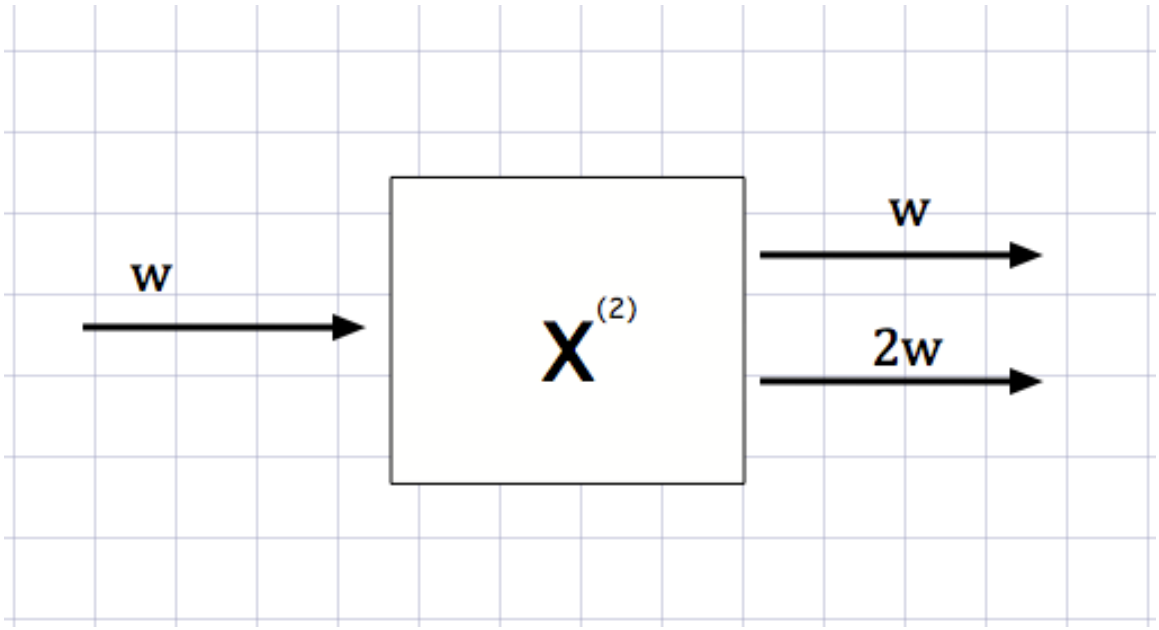

Figure 4. An incident wave of frequency ω propagates in a second order nonlinear medium inducing an emission wave of frequency 2ω.

When a 1064 nm continuous-wave laser hits the crystal inside the second harmonic generator, the electric field of the incident infrared light interacts with the second order nonlinear crystal. As a result of this interaction as we saw above, a second harmonic wave is created, which produced green light at twice the optical frequency of the incident infrared light.

II. Intra-Cavity Loss Characterization:

The second harmonic generator was assembled without the crystal inside in order to be able to measure the intra-cavity loss. In the past, one of our SHGs failed after operating thousands of hours, so we investigated the intra-cavity losses. After having built the SHG, we designed the optical setup as shown in Figure 5, and we placed each

component on the optical table. Then, we aligned the laser and measured the waist size of the beam by using a beam profiler. We used the beam splitter that is located before the first mirror in Figure 5 as our reference point, and we found the waist size to be 132.5 μm.

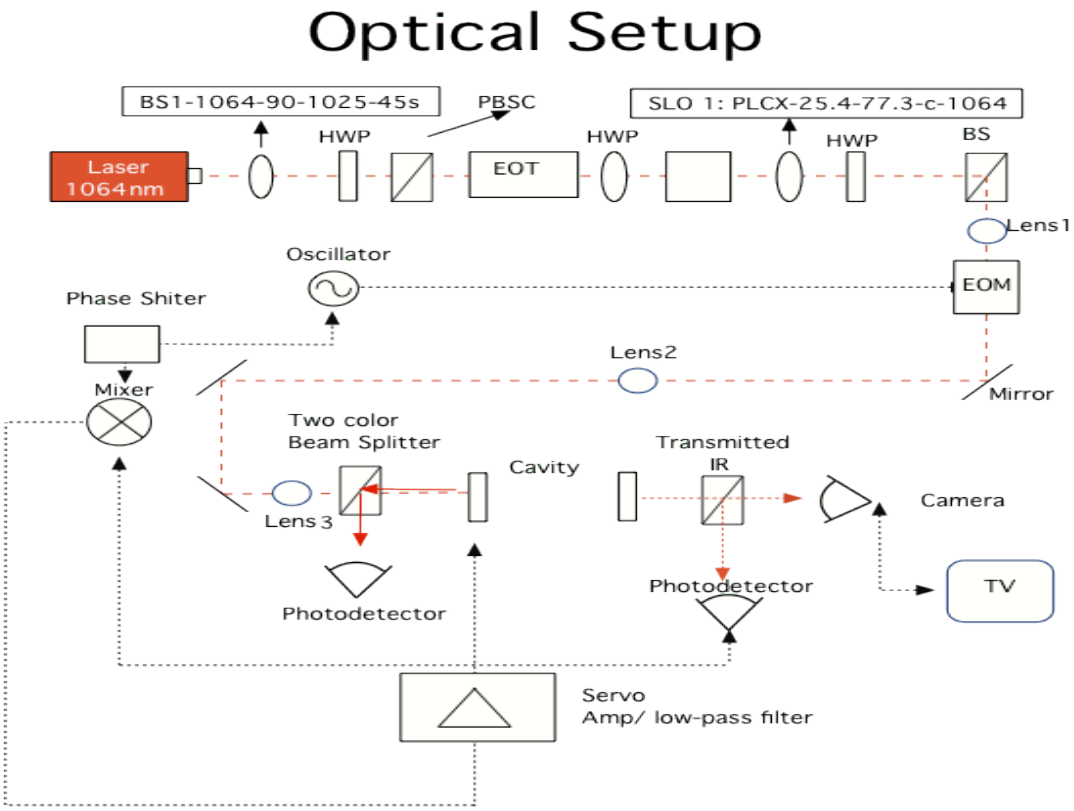

Figure 5. Optical layout, the black dashes represent the Pound-Drever-Hall (locking) technique.

After obtaining the waist size that the laser has, we needed to know the size of the waist that we needed inside the SHG. Since the SHG is a Fabry-Perot cavity with two mirrors of the identical curvature, the waist inside the cavity is given by $w_0^2 = \frac{L\lambda}{\pi}\sqrt{\frac{g}{1-g}}$, where ω_o is the waist size, L is the length of the cavity, and g is the resonator parameter; by definition $g = 1 - \frac{L}{R}$, where R is the curvature of the mirrors. Using this formula, we found that the waist of our cavity is 63 μm. Using the information about the waist size

needed inside the cavity and the actual waist size that the laser has, we calculated the position where the lenses need to be placed on the optical table as shown in Figure 6.

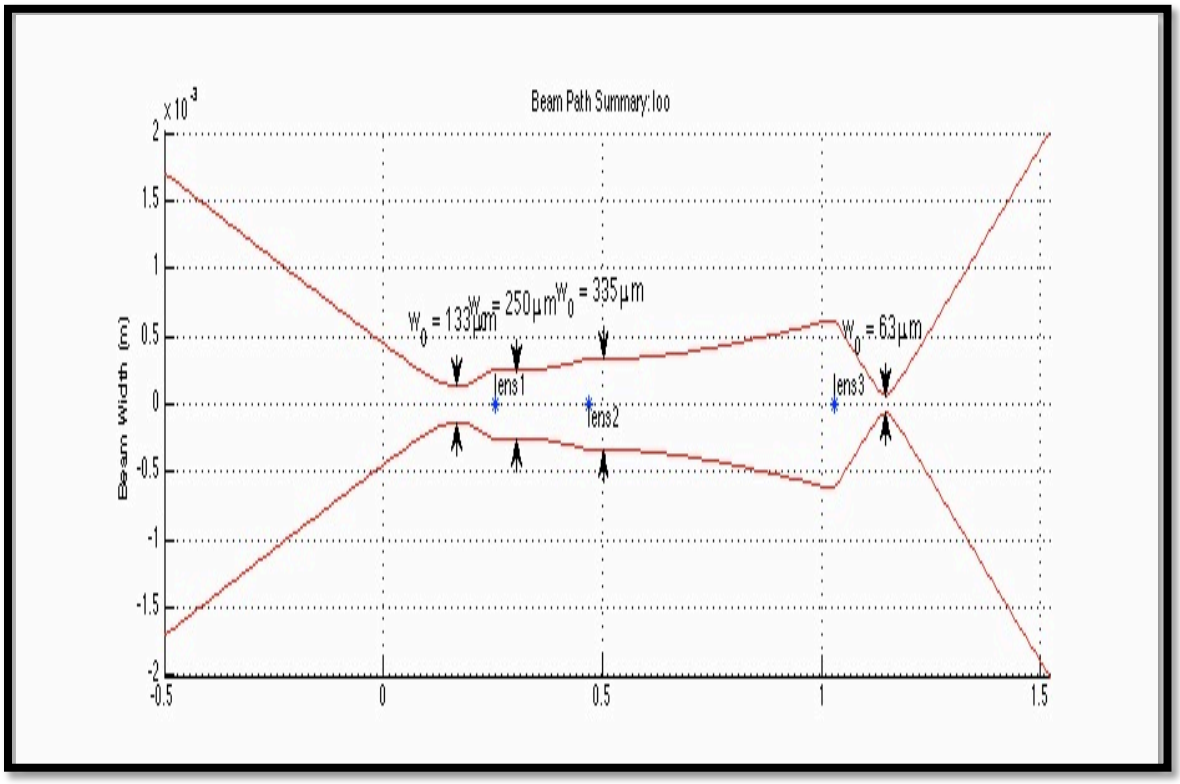

Figure 6. Beam width versus distance away from the beam Splitter.

We placed the cavity in the same position as shown in Figure 6. Then, we aligned the laser with the cavity. The intra-cavity loss can be found by using this formula

$$\frac{I_{r-on-resonance}}{I_{r-off-resonance}} = \frac{\left[\frac{r-r_l}{1-rr_l}\right]^2}{\left[\frac{r+r_l}{1+rr_l}\right]^2}$$, where r is the reflectivity of the mirror, I is the photocurrent measured by the photodetector or the reflect power from the cavity, and the formula $IntraCavityloss = 1 - r_l^2$. We measured the intra-cavity loss, and we found an intra-cavity

loss of 4.70% without the crystal, which is surprisingly high, since we were expecting a loss of less than 1%.

III. Locking the Cavity to the Laser and its Characterization:

The cavity will be locked to the laser on the fundamental TEM_{00} mode by using the Pound-Drever-Hall method. A basic diagram of the Pound-Drever-Hall method is illustrated in Figure 7.

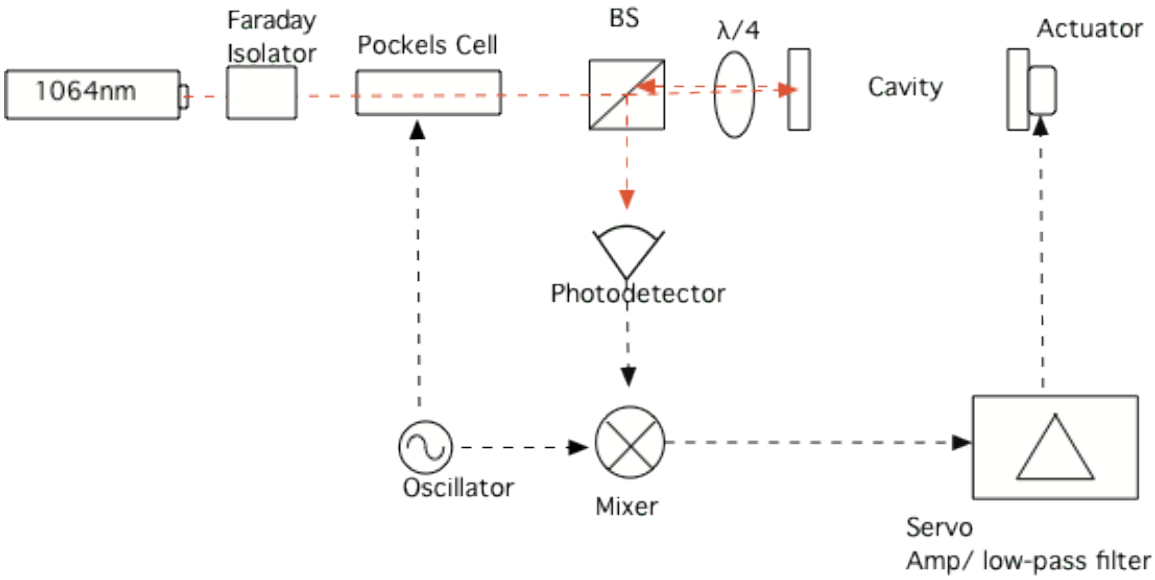

Figure 7. The basic Pound-Drever-Hall layout for locking the cavity to the laser.

In Figure 7, a 1064 nm laser is sent to a cavity. The faraday isolator prevents the reflected beam from retroreflecting back to the laser and destabilizing it. The beam splitter and the quarter wave plate convert linear polarized light into circular polarized light. The photodetector takes the reflection light and its output goes into a mixer. The mixer's output goes to the PZT, an actuator control the length of the cavity. By using a feedback control system, the cavity can be locked on resonance.

Before locking the cavity, we measured the mode mismatch by scanning the cavity and measuring the ratio of the height of the 00 peak to the mode mismatch peaks. The mode mismatch resonating inside the cavity are 20, 02, and 11 modes, which modes are shown in Figure 8. We measured a mode mismatch of 10.58% as shown in Figure 9.

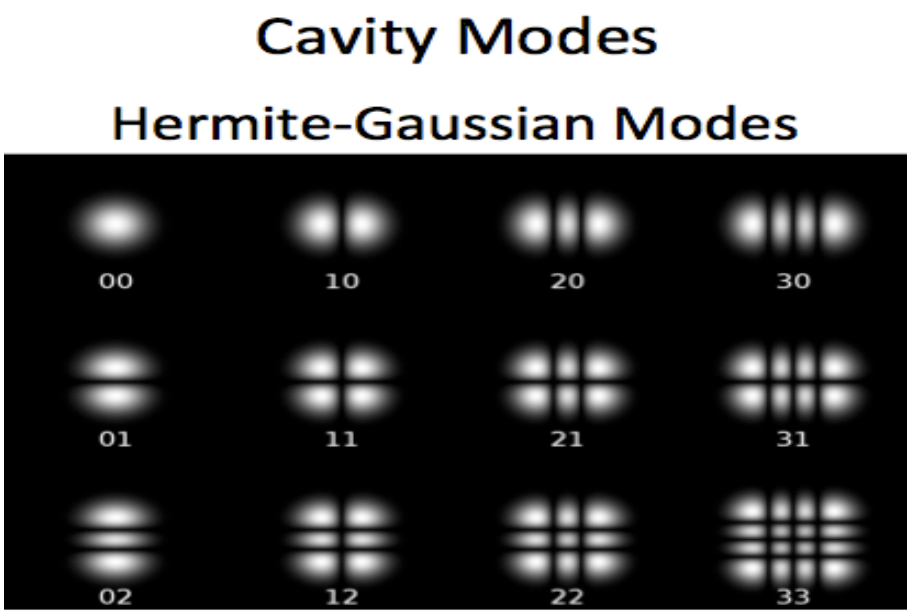

Figure 8. Hermite Gaussian Modes [8]

Figure 9. The yellow signal is the transmitted signal, and the higher two peaks in this graph is the 00 peak and the other three small peak are 20, 02 and 11 modes respectively.

For our Pound-Drever-Hall method, we are not using the reflected light but instead we are using the transmitted light. We are using the transmitted light because the second harmonic generation required linear polarization. Because we are using transmitted light for the Pound-Drever-Hall method, the sidebands are been introduced inside the cavity, which adds some phase noise to the circulating field inside the cavity. In Figure 5, the EOM is the phase modulator. The signal from the oscillator is used to drive the EOM, and it is used at the mixer to demodulate the signal from the photodetector. The output of the mixer is the error signal, which is proportional to the cavity length. The mixer takes the output of the photodetector, which is connected to the servo. This error signal is used by a servo controller. Inside the cavity, there is a PZT, which is equivalent to an actuator in Figure 7. Using the Pound-Drever-Hall method, we were able to lock the cavity as showing in Figure 10.

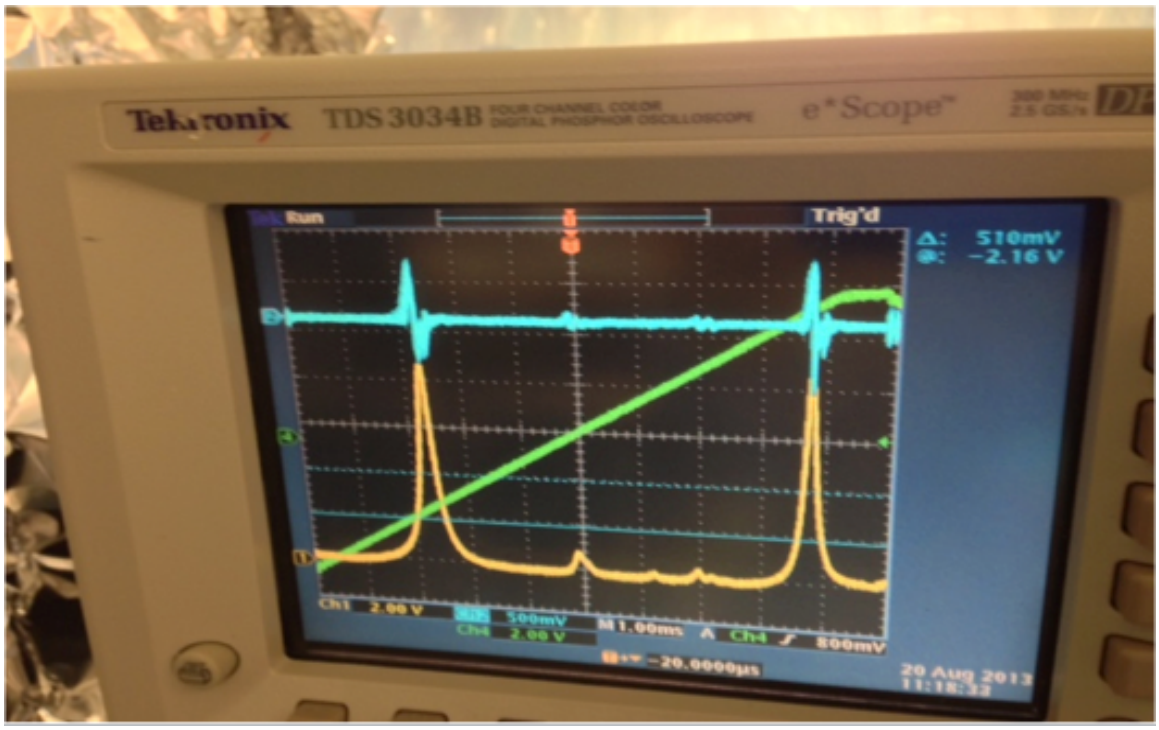

Figure 10. This is the Pound-Drever-Hall method in a Fabry-Perot cavity. The blue signal represents the Pound-Drever-Hall error signal. The yellow signal represents the transmitted signal.

After locking the cavity to the laser, we now need to characterize how well our locking works. In order to characterize it, we are going to use a spectrum analyzer. We are going to look at the transfer function of the open loop gain by using the spectrum analyzer, and we are going to see the frequency response of the PZT. We used the open loop transfer function to be able to characterize the lock performance and stability by looking at how much noise gets suppressed as a function of frequency. For the open loop gain, we are expected to observe a low pass filter. In order to characterize the system, we injected noise into the system using the spectrum analyzer, and we measured how the system reacted to the noise. We are interested in the unity gain frequency of the open loop transfer function and on the phase unity gain frequency, which tells us how stable the loop is. The further away the phase unity gain frequency is from 180° in the open loop the more stable the system is. Figure 11 illustrates the open loop gain, which has a low pass filter as we expected for the magnitude of the transfer function, and the phase is less than 180°, which tells us that the locking is stable. For the PZT frequency responses, we expected to observe constant amplitude until the resonance frequency, which occurs between10kHz to 20kHz. Figure 12 illustrates the frequency response of the PZT and as expected the frequency is constant until the resonance frequency, around 10kHz. The measurement illustrates that our locking is working well.

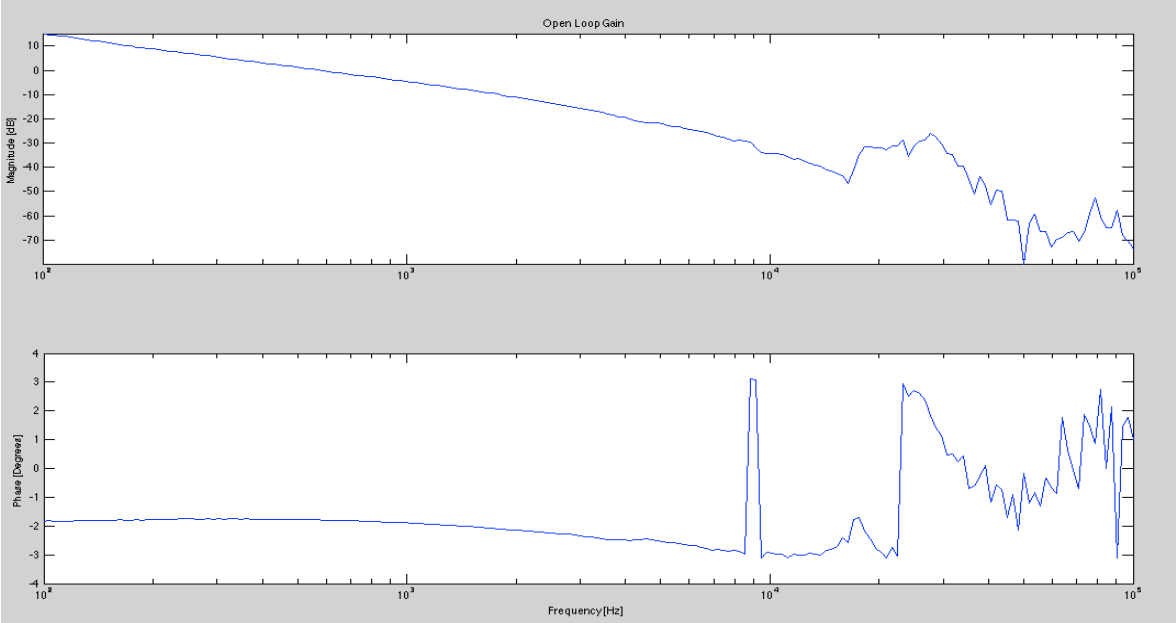

Figure 11. Cavity Open Loop Gain frequency response

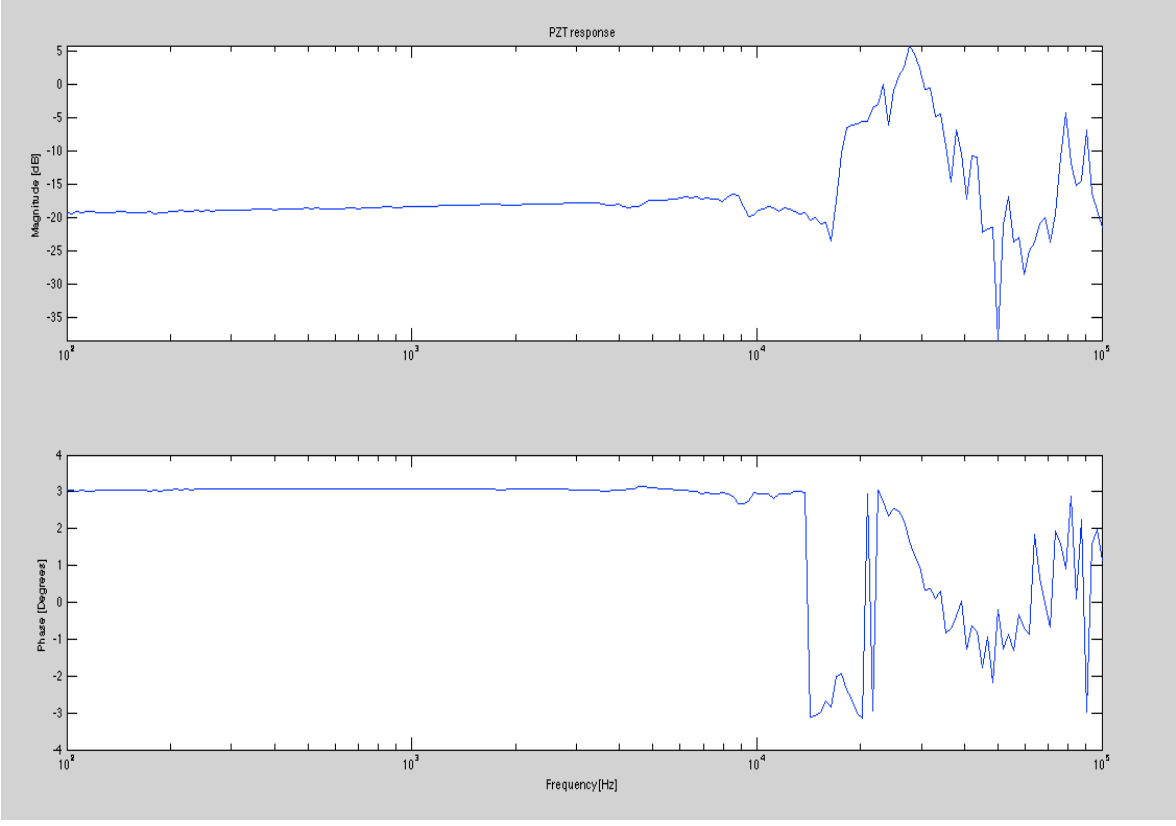

Figure 12. PZT frequency response

IV. Phase Matching and Conversion Efficiency

After characterizing the cavity locking, we placed the crystal inside the cavity. Before we look at the conversion efficiency, we need to first take a look at the phase-matching condition in our cavity. From the previous sections we know that when an electric field is applied to a second order nonlinear crystal, the incident electric field induces an electric field inside the crystal. This induced electric field is twice the frequency of the incident electric field. As the incident electric field propagates through the nonlinear dielectric material, there is a continuous generation of electric fields as shown in Figure 13. In Figure 13, an electric field is applied to a non-centrosymmetrical crystal, which results in second harmonic generation. The generated electric field at time T interacts with the electric field generated at time 2T and so on. This interaction between the generated electric fields can be either constructive or destructive.

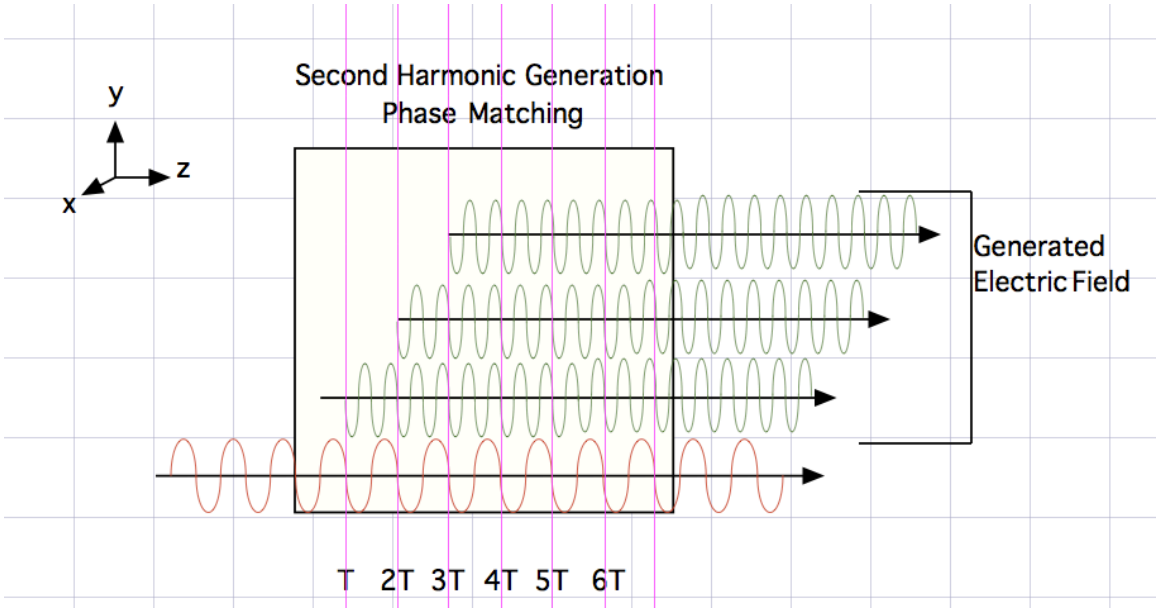

Figure 13. A monochromatic wave of frequency ω propagates inside a non-centrosymmetrical crystal in the z direction. This results in second harmonic generation, where a field of frequency 2ω is generated. The generated field interacts by either constructive or destructive interference.

As we can see in Figure 13, we would like the generated electric field to interact constructively because this will result in the greater conversion efficiency. In other words, the phase matching condition is an important factor when looking at the conversion efficiency in a SHG.

Let's assume that we have an electric field $\mathbf{E_1}(\omega)$ and $\mathbf{E_2}(2\omega)$ propagating inside crystals in the z direction and whose electric fields are given by the following formulas:

$$\boldsymbol{E_1}(\omega, z) = \boldsymbol{a_1} A_1(z) e^{ik_1 z} \tag{4.1}$$

$$\boldsymbol{E_2}(2\omega, z) = \boldsymbol{a_2} A_2(z) e^{ik_2 z} \tag{4.2}$$

where $\mathbf{a_1}$ and $\mathbf{a_2}$ are the unit vectors along the light polarization and $A_1(z)$ and $A_2(z)$ are the amplitude functions and k_1 and k_2 is the wave vector [2]. The nonlinear polarization vector associated with these two given electric fields will be as follow:

$$\mathbf{P^2}(\omega, z) = \varepsilon_0 \chi^{(2)}(2\omega, -\omega) \boldsymbol{E_2 E_1^*} = \varepsilon_0 \chi^{(2)}(2\omega, -\omega) \boldsymbol{a_2 a_1}^* A_2(z) A_1^*(z) e^{i(k_2 - k_1)z} \tag{4.3}$$

$$\mathbf{P^2}(2\omega, z) = \varepsilon_0 \chi^{(2)}(\omega, \omega) \boldsymbol{E_1^2} = \varepsilon_0 \chi^{(2)}(\omega, \omega) \boldsymbol{a_1^2} A_1^2(z) e^{2ik_1 z} \tag{4.4}$$

By using the coupled-wave equation and the slowly varying amplitude approximation, we have the following equation [2]:

$$\frac{\partial \mathrm{A}(\omega,z)}{\partial \mathrm{z}} = \frac{\mathrm{ik}}{2\varepsilon(\omega)} [\boldsymbol{a_0} \cdot \boldsymbol{P^{NL}}(\omega, z)] e^{-ikz} \tag{4.5}$$

where $\mathbf{P^{NL}}$ is the nonlinear polarization vector. By taking equation 4.5 in terms of the $A_2(z)$ and substituting equations 4.4 into it, we would obtain the following results:

$$\frac{\partial A_2(\omega,z)}{\partial z} = \frac{ik_2}{2\varepsilon(2\omega)} \left[\boldsymbol{a_2} \cdot \boldsymbol{P^{(2)}}(\omega, z)\right] e^{-ik_2 z} \tag{4.6}$$

$$= \frac{ik_2 \varepsilon_0}{2\varepsilon(2\omega)} \left[\boldsymbol{a_2} \cdot \left(\boldsymbol{a_1^2} \chi^{(2)}(\omega, \omega) A_1^2(z) e^{2ik_1 z}\right)\right] e^{-ikz} \tag{4.7}$$

$$= \frac{ik_2 \varepsilon_0}{2\varepsilon(2\omega)} \left[\boldsymbol{a_2} \cdot \boldsymbol{a_1^2} \chi^{(2)}(\omega, \omega)\right] A_1^2(z) e^{i(2k_1 - k_2)z} \tag{4.8}$$

from equation 4.8, we can define the phase mismatch factor as follows:

$$\Delta k = 2k_1 - k_2 = \frac{4\pi}{\lambda_1}[n(\omega) - n(2\omega)] \quad (4.9)$$

where λ_1 is the wavelength of the fundamental wave (or the wavelength of the incident wave). Equation 4.8 tells us that the larger Δk is, the smaller the amplitude will be, which results in less intensity because intensity is the square of the amplitude. The phase matching condition is when Δk=0, so 2n(ω)=n(2ω)

From the phase mismatch expression that we obtained in Equation 4.9, we know that n(ω)≠n(2ω) because the index of refraction is a function of frequency. However, in birefringent materials, the phase matching condition of 2n(ω)=n(2ω) is possible since materials that displayed birefringence have different indices of refraction for different polarization. There are three different methods or techniques that could be used in order to achieve the phase matching condition: 1) type I phase matching, 2) type II phase matching, and 3) quasi phase matching. Since the crystal that we are using is potassium titanyl phosphate (KTP), we would use quasi phase matching techniques. In the case of using quasi phase matching, we would have an expression for the mismatch Δk as following[4]:

$$\Delta k = m\frac{2\pi}{\Lambda} - (k_2 - 2k_1) = 0$$

where Λ is the period in which the positive c axis of the crystal alternates in orientation and m is an integer. By plotting the amplitude of the generated fields versus the distance that the fields propagate inside the crystal, in Figure 14, we can observe how quasi phase matching give us an increasing amplitude. In Figure 14, we can observe that perfect phase matching grows linearly as the generated field propagates through the crystal. However, as the generated fields propagate through the crystal in the presence of phase

mismatching, the net electric field behaves as a sinusoid with small amplitude. In the case of quasi phase matching, we can observe that when the amplitude is about to decrease as a result of phase mismatch, the nonlinear coupling coefficient d_{eff} changes its sign, which results in the amplitude of the generated electric fields to increase monotonically [2].

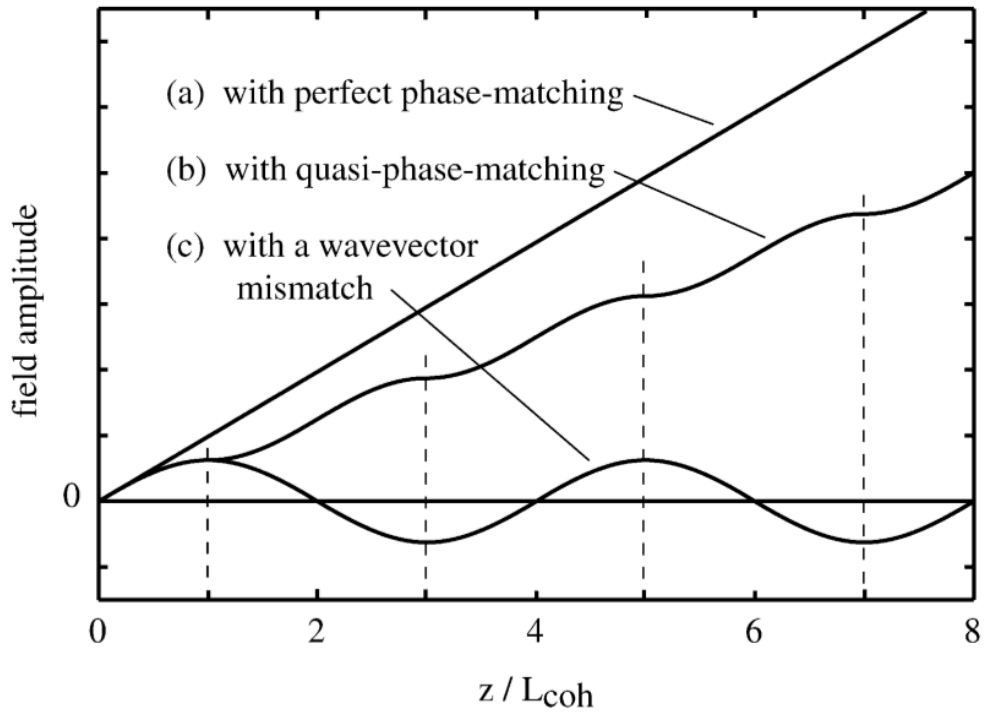

Figure 14. a) When perfect phase matching condition is satisfied the amplitude of the field increase linearly. b) In the case of quasi phase matching, the amplitude increases monotonically. c) In the case of phase mismatch, a sine wave with small amplitude. [3].

The quasi phase matching does not display a linear fast increase as perfect phase matching, but it displays a monastically linear that does not allow phase mismatch.

Phase matching can be accomplished by two different methods: 1) by angle tuning and 2) by temperature tuning. In this experiment, we are going to accomplish phase matching by using temperature tuning. Before we experimentally measure the phase matching at different temperature, we first simulated it using Matlab in order to

know what to expect. Figure 15 illustrated the prediction of the phase matching as the temperature is varied.

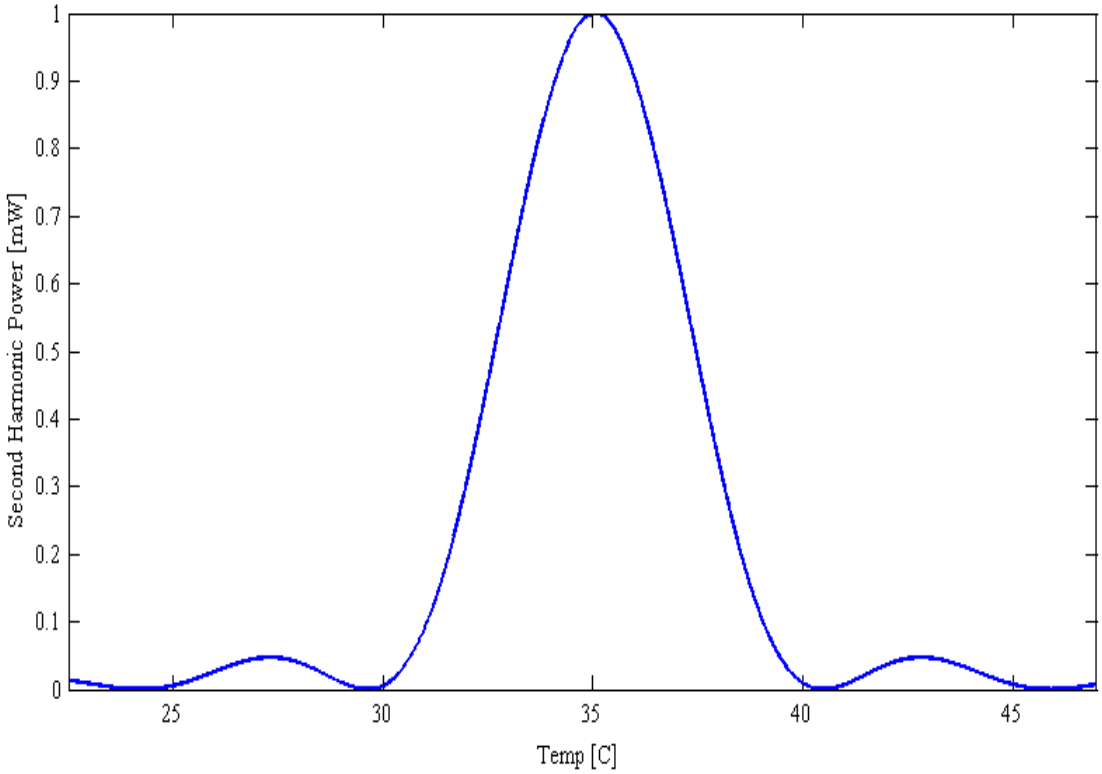

Figure 15. Normalized prediction of the phase matching curve

In Figure 15, we obtained that the maximum power intensity will be obtained at 35°C. In order to measure the phase matching curve, we are going to use a photon detector and an oscilloscope to measure the power of the green light. As we changed the temperature by small steps, we recorded the voltages for the different temperatures. Then, we plotted voltage versus temperature, and we obtained a temperature of 33°C for the maximum voltage as shown in Figure 16. Our measurements of the phase matching curve agrees with our prediction.

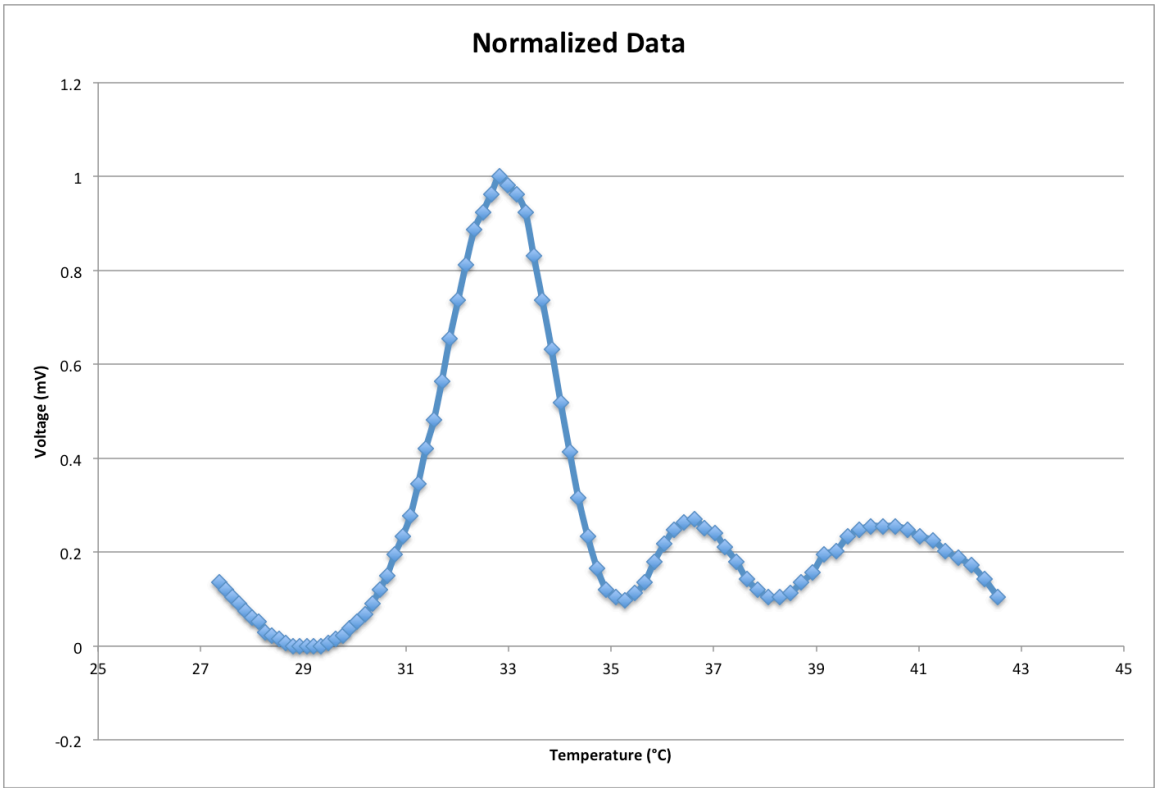

Figure 16. Obtained Phase Matching Curve at an incident infrared power of 15.33mW

After characterizing the phase mismatch, let's take a look at the conversion efficiency of our second harmonic generator. The conversion efficiency will be given by

$$\eta_{SHG} = \frac{P_{532}}{P_{1064}}$$

This will meaning that increasing the power of the incident infrared light will result in an increase in the power of the generated green light. We measured the power of the incident infrared and the power of the green light, and we found a conversion efficiency of 27% at an incident power of 100mW. Since the conversion efficiency increases with increase of the power, we expected to obtain higher conversion efficiency. In Figure 16, we measured the power of the green light from three different incident infrared powers. We calculated the conversion efficiency, and then we fitted to a curve as shown in Figure 17. This graph below tell us that we could obtained a conversion efficiency of about 45% if

we use half of a Watt. This means that having an incident infrared of power of 500mW would give us a green light power of 225mW, which is good enough for Advance LIGO.

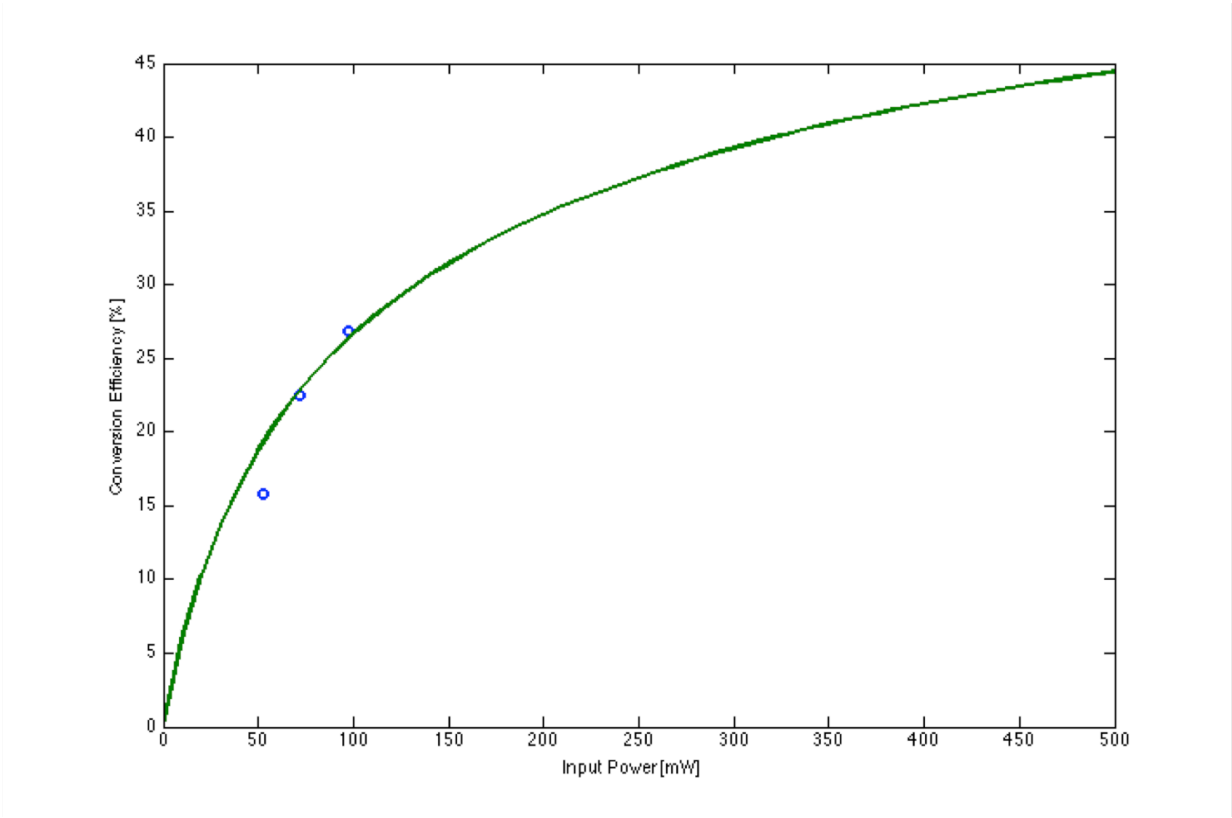

Figure 17. Conversion efficiency versus input power. The three circle dots in the graph represent the measured data, and the green curve is the fitted curve that predicted the conversion efficiency with increase input power.

V. Conclusions

In this paper, we characterized the second harmonic generation by looking at the intra-cavity losses, the stability and locking of the cavity, and the conversion efficiency. We found an intra-cavity loss of 4.70%, which is bigger than what we expected it to be. We looked at the locking and the stability of the cavity by looking at the open loop gain

of the system and the frequency response of the PZT, and the we found that the cavity is working well and its locking is stable for the experiment. The conversion efficiency seems promising since we got 27%, which the conversion efficiency curve tell us that we could potentially obtained a 45% of conversion efficiency by just increasing the incident power. However, if we reduce the mode mismatch by aligning the cavity better, we could potentially obtain higher conversion efficiency. For future experiments, we need to measure the conversion efficiency when the laser run over thousands of hours in order to characterize the reduction in conversion efficiency over a long timescale.

Reference

[1] Aasi, J., et al. "Enhanced sensitivity of the LIGO gravitational wave detector by using squeezed states of light." *Nature Photonics* 7 (2013): 613-619.

[2] Boyd, Robert W., *Nonlinear Optics*., Burlington: Elsevier, 2008.

[3] Boyd, Robert W. "Nonlinear Optics." Infographic. *Nonlinear Optics*. By Boyd. Burlington: Elsevier, 2008. 86. Print.

[4] Goda K 2007 Development of techniques for quantum-enhanced laser-interferometric gravitational-wave detectors PhD Thesis Massachusetts Institute of Technology, Cambridge < https://gwic.ligo.org/thesisprize/2007/Goda_Thesis.pdf >

[5] He, Guang S., Liu, Song H., *Physics of Nonlinear Optics*, World Scientific Publishing Co., Farrer Road, 1999.

[6] *LIGO Advanceligo Extending the Physics Reach of LIGO*. N.p., 15 Oct. 2012. Web. 15 Apr. 2014. <https://www.advancedligo.mit.edu/summary.html>.

[7] McClelland, D.E., Mavalvala, N., Chen, Y., Schnabel, R., *Advance Interferometry, Quantum Optics and Optomechanics in Gravitational Wave Detectors*, *Laser &* Photonics Reviews 5.5 (2011): 677-696.

[8] *Optique Pour L'ingénieur Ressources Numériques*. Free Software Foundation, <http://www.optique-ingenieur.org/en/courses/OPI_ang_M01_C03/co/Contenu_13.html>

[9] Schnabel, R., Mavalvala, N., MacClelland D.E., & Lam, P.K., *Quantum metrology for gravitational wave astronomy*, Nature Communications 1 (2010): 121.